Remote Sensing of Environment 76 (2000) 139–155

Remote Sensing of Environment

www.elsevier.com/locate/rse

Land cover mapping in an agricultural setting using multiseasonal Thematic Mapper data

Doug R. Oetter[a], Warren B. Cohen[b,*], Mercedes Berterretche[a], Thomas K. Maiersperger[a], Robert E. Kennedy[a]

[a]Department of Forest Science, Oregon State University, Corvallis, OR, USA
[b]Forestry Sciences Laboratory, Pacific Northwest Research Station, USDA, Forest Service, 3200 SW Jefferson Way, Corvallis, OR 97331, USA

Received 13 June 2000; accepted 18 October 2000

Abstract

A multiseasonal Landsat Thematic Mapper (TM) data set consisting of five image dates from a single year was used to characterize agricultural and related land cover in the Willamette River Basin (WRB) of western Oregon. Image registration was accomplished using an automated ground control point selection program. Radiometric normalization was performed using a semiautomated approach based on the identification of no-change pixels in forest, urban, and water classes. Reference data were developed using existing data sets, including low-level 35-mm color slide photographs, 1:24,000 color airphotos, and ancillary geographic information system (GIS) coverages. Preliminary examination of the data structure included plotting of training set temporal trajectories in spectral space with reference to existing crop calendars. A subsequent stratified, unsupervised classification algorithm, in combination with a geoclimatic rule set and regression analysis, was used to label mapped cells. A map of 20 land cover classes was developed. Classes included agricultural crops and orchards, forest and natural cover types, and urban building densities. An accuracy assessment indicated a final map error of only 26%. The map is now being used to model present and future landscapes for the basin.

Keywords: Landsat Thematic Mapper; Land cover mapping; Crop cover mapping; Farm Service Agency; Tasseled Cap; Willamette Valley

1. Introduction

The Pacific Northwest region of the US has been a major focus for resource-related issues throughout the 1990s (Tuchmann, Connaughton, Freedman, & Moriwaki, 1996; United States Department of Agriculture, 1993). Recent debates have centered around the effects of forest management on survival of late successional forest dwelling species and on fish habitat. These and related topics were addressed in the President's Northwest Forest Plan (Tuchmann et al., 1996). In direct response to the Plan, the Pacific Northwest Ecosystem Research Consortium (PNW-ERC) was formed by the Environmental Protection Agency (EPA) in 1994. The PNW-ERC consists of 13 individual projects with the common research goal of understanding "... ecological consequences of possible societal decisions related to changes in human populations and ecosystems in the Pacific Northwest and [developing] transferable approaches and tools to support management of ecosystems at multiple spatial scales" (Environmental Protection Agency, 1997).

An important data layer required by the PNW-ERC was a land cover map of the Willamette River Basin (WRB). The land cover map would be used both as a baseline to document current ecological conditions and as a base for projections of alternative future landscapes. The PNW-ERC projects required a high-resolution land cover map for the study area (Fig. 1), which would characterize the wide variety of natural and anthropogenic microenvironments, including detailed information about forest condition, agricultural practices, and urban development. The framework for the PNW-ERC research was based on an initial pilot study of the 23-km^2 Muddy Creek watershed in Benton County, OR (Hulse et al., 1999). That study identified 30 land use/land cover types using 1:24,000 aerial photographs and ancillary information, and served as a potential model for the land cover map of the entire basin.

* Corresponding author. Tel.: +1-541-750-7322; fax: +1-541-758-7760.
E-mail address: cohen@fsl.orst.edu (W.B. Cohen).

0034-4257/00/$ – see front matter
PII: S0034-4257(00)00202-9

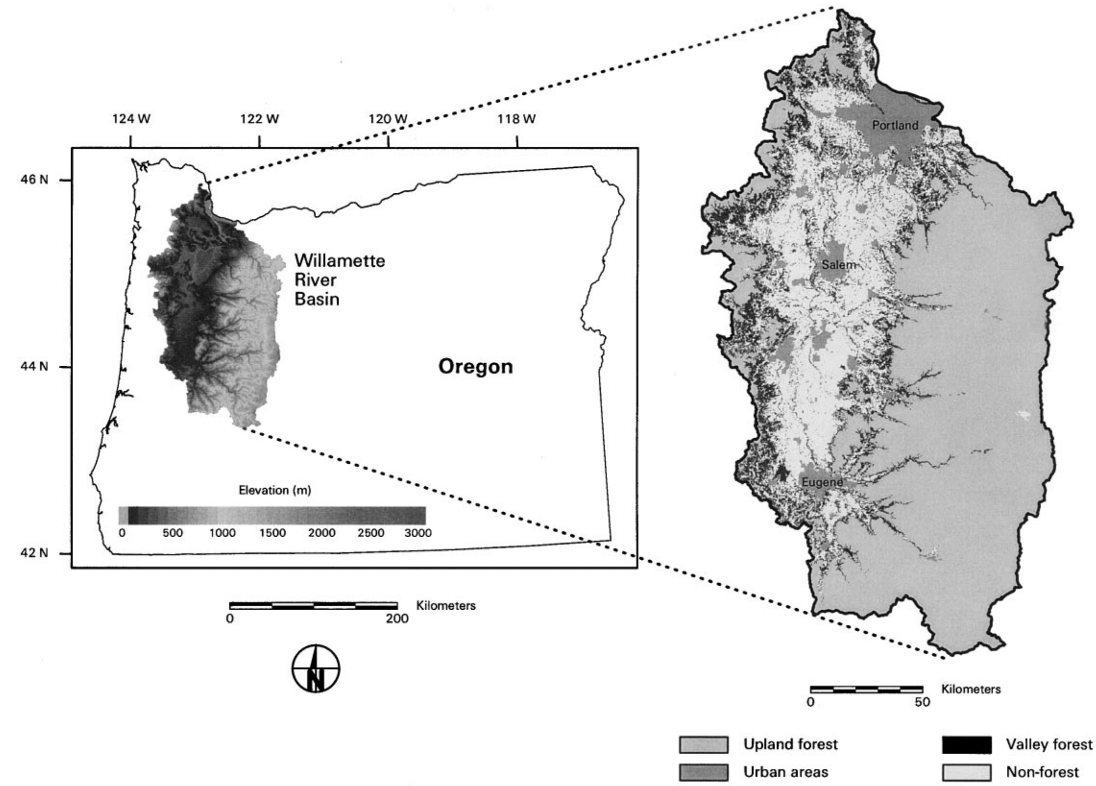

Fig. 1. The WRB in northwest Oregon. The Willamette River drains north from Eugene to Portland, where it joins with the Columbia River. Inset on left shows elevation. Blowup at right shows the basin divided into four mapping units that define the steps used to complete mapping of the basin.

We referred to a large literature on the use of Thematic Mapper (TM) data for land cover mapping, especially for the land cover types that we were asked to identify: agricultural crops (Bauer, Hixson, Davis, & Etheridge, 1978; Buechel, Philipson, & Philpot, 1989; Shueb & Atkins, 1991), grasslands (Lauver & Whistler, 1993), riparian areas (Hewitt, 1990), and urban cover (Haack, Bryant, & Adams, 1987; Plunk, Morgan, & Newland, 1990). Our previous work had been focused on single-date TM data for forest cover mapping (Cohen, Spies, & Fiorella, 1995; Cohen, Maiersperger, Spies, & Oetter, 2001) and forest cover change detection using multiyear Landsat data (Cohen & Fiorella, 1998; Cohen, Fiorella, Gray, Helmer, & Anderson, 1998). In this study, we followed the lead of many other researchers who have recognized the benefits of using multiseasonal imagery (within a given year) to map crops (Brewster, Allen, & Kopp, 1999; Brisco & Brown, 1995; Ehrlich, Estes, Scepan, & McGwire, 1994; Lo, Scarpace, & Lillesand, 1986; Panigrahy & Sharma, 1997; Pax-Lenney & Woodcock, 1997; Pax-Lenney, Woodcock, Collins, & Hamdi, 1996; Ryerson, Dobbins, & Thibault, 1985; Williams, Philipson, & Philpot, 1987), grasslands (Henebry, 1993), forests (Schriever & Congalton, 1995; Wolter, Mladenoff, Host, & Crow, 1995), and wetlands (Lunetta & Balogh, 1999; Munro & Touron, 1997). In addition, we elected to augment our remotely sensed data with ancillary geographic information system (GIS) data (Adinarayana, Flach, & Collins, 1994; Carbone, Narumalani, & King, 1996; Ehrlich et al., 1994; Zhuang, Engel, Baumgardner, & Swain, 1991) and a digital elevation model (DEM) (Henebry, 1993).

Since the upland forest portion of the WRB had previously been mapped (Cohen et al., 2001), our task was to map the valley floor, which we defined as a contiguous area of $\leq$315-m elevation. Our objectives for this study were to use multiseasonal Landsat TM data (1) to produce a land cover map of the valley floor that would, to the extent possible, match a list of desired classes for agricultural, forest, natural, and urban cover types (Table 1), and (2) to extend our working knowledge of the Tasseled Cap transformation (Crist & Cicone, 1984) into an agricultural setting. The resultant land cover map incorporates the advantages of multiseasonal satellite imagery and GIS information to map relatively detailed cover types across the Willamette Valley.

1.1. Study area

The WRB occupies a 29,740-km^2 region in northwest Oregon bounded by the mountains of the Coast Ranges and the Cascade Range (Willamette Valley Livability Forum, 1999). Over 2 million people inhabit the basin, primarily in the metropolitan areas of Portland, Eugene, and Salem. Although the basin contains only 12% of the State's land

Table 1
Categorical list of the land cover/land use classes desired by the PNW-ERC

1. Urban
- a. Residential
  - i. 0–8 dwellings/acre
  - ii. 9–16 dwellings/acre
  - iii. ≥17 dwellings/acre
- b. Commercial
- c. Industrial
- d. Open space
- e. Herbaceous-roads

2. Built (nonurban)
- a. Commercial
- b. RR2-5 zoning
- c. Within 2 acres of structures
- d. Railroad
- e. Roads
  - i. Primary roads
  - ii. Secondary highway
  - iii. Light duty road
  - iv. Unimproved road
- f. Revetments

3. Hydrology
- a. Headwater streams
- b. Open-standing water
- c. Streams > first order

4. Forest
- a. 0–40-year-old Douglas fir
- b. 41–120-year-old Douglas fir
- c. >120-year-old Douglas fir
- d. Mixed conifer/deciduous
- e. Deciduous
- f. Lower riparian forest

5. Agriculture
- a. Grass seed/grain
- b. Hybrid poplar
- c. Nursery operations
- d. Orchards
- e. Pasture and haylands
- f. Row crops
- g. Vineyards, berries, and hops
- h. Christmas trees
- i. Mint
- j. Meadowfoam
- k. Confined animal operations
- l. Farmsteads

6. Open/woody
- a. Shrub/brush
- b. Fence rows
- c. Oak savanna
- d. Prairie (grass/forb)
- e. Marsh (nontreed wetlands)

7. Percent impervious surface
- a. < 10%
- b. 10–20%
- c. >20%

The research effort required a fine-detailed map of many different microenvironments.

area, it accounts for over 50% of its $3.5 billion agricultural economy (ODA, 1999). In addition, the basin supports a thriving forest product industry, primarily due to highly productive Douglas fir forests.

The WRB consists of three physiographic provinces: the Coast Ranges, Willamette Valley, and Western Cascades (Franklin & Dyrness, 1988). The dominant natural vegetation of the volcanic and sedimentary Coast Ranges includes *Thuja plicata* (western red cedar), *Tsuga heterophylla* (western hemlock), and *Pseudotsuga menziesii* (Douglas fir). The volcanic Western Cascades montane province contains mixed conifer forests, primarily Douglas fir and western hemlock. Both provinces have substantial *Acer macrophyllum* (bigleaf maple) and *Alnus rubus* (red alder) hardwood stands in disturbed areas. The Willamette Valley contains alluvial terraces and floodplains interrupted by rolling hills of volcanic and sedimentary origin. The natural vegetation of this area consists of riparian hardwood forests, wet and dry prairie grasslands, herbaceous transition areas, *Quercus garryana* (Oregon white oak) woodlands, and mixed conifer remnant forests (Franklin & Dyrness, 1988; Johannsen, Davenport, Millet, & McWilliams, 1970; Towle, 1982; John Christy, personal communication).

The WRB has a cool Mediterranean climate (Jackson & Kimerling, 1993). The valley floor averages 100–125 cm of annual precipitation, while the Coast Ranges and the Cascades get much more, with averages up to 300 cm. Average temperatures on the valley floor range from a mean January minimum of 1°C to a mean July maximum of 30°C (Oregon Climate Service, 1999). Elevation in the basin varies from 15 to 3200 m amsl (Willamette Valley Livability Forum, 1999).

While timber extraction is the main industry in the upland forests of the basin, agriculture dominates the valley floor. Because of the rich alluvial soils and the temperate climate, the Willamette Valley supports over 120 different crops (ODA, 1999). Depending on soil type and location, commodities range from exotic fruits and vegetables to a variety of grains and nuts (Daryl Ehrensing, personal communication). The leading products include nursery and greenhouse stock, seed crops, Christmas trees, fruit and nut crops, and peppermint (ODA, 1999).

2. Methods

2.1. Remotely sensed imagery and preprocessing

The TM scenes used in this study included multiple rows (28–30) in path 46 (EROS Data Center; Sioux Falls, SD). We selected 1992 because ground and airphoto reference data from 1992 and 1993 were available. Moreover, that was a dry year in the valley, and five nearly cloud-free TM image data sets from one growing season were available. The dates of the TM images were March 19, May 6, June 7, July 25, and August 26 (Fig. 2). Each date of imagery

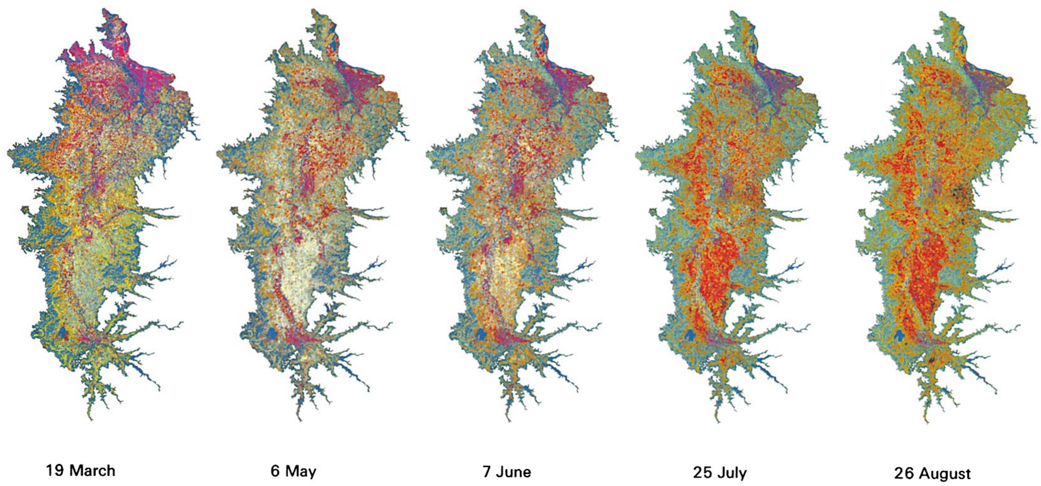

Fig. 2. Landsat TM images acquired in 1992. Each image is a multiple scene combination of Rows 28, 29, and 30 from path 46, shown in the Tasseled Cap transformation (brightness, greenness, and wetness in red, green, and blue, respectively).

covered all three consecutive rows from the same path and captured the entire study area. As such, imagery from each date could be treated as a single spectral data set for processing purposes. These five dates represent the near full progression of phenological development of the major crops grown in the valley, which is critical for the accurate classification of agricultural land cover types (Pax-Lenney & Woodcock, 1997). All images were of excellent quality, and only the June image contained clouds confined to small areas in the northwest corner of the scene.

Because we intended to analyze changes in Tasseled Cap vegetation indices among the five different imagery dates to identify land cover types, georegistration and radiometric normalization of the images were performed. Georegistration was accomplished in two steps. First, we registered the four other images to the June 7 image using an affine transformation. Second, all five images were resampled to match a geocoded TM base image mosaic from 1988 using a second-order polynomial nearest-neighbor transformation. To select the points used to build the transformation matrix (tie points), we employed a program developed by Kennedy and Cohen (Pers.comm.). The procedure locates tie points by maximizing an index of normalized cross-correlation for small subsets of the two images to be matched. A minimum of 150 points for each image provided a second-order polynomial transformation with less than one-half pixel root mean square (RMS) error.

Our radiometric normalization procedure was based on the approach of defining radiometric control sets along a brightness gradient from very dark (e.g., water and forest) to very bright (e.g., urban) using colocatable pixels. Rather than selecting colocated control sets manually in both the "subject" and "reference" images (e.g., Eckhardt & Verdin, 1990; Vogelmann, 1988), we elected to use "difference-image" space to capture the control set of no-change pixels. We first created difference images (Coppin & Bauer, 1996) by subtracting the subject image from the June 7 reference image for each of the six reflectance bands. We then added Band 4 from the June 7 image as a baseline against which spectral differences could be contrasted (see Cohen & Fiorella, 1998). Each of these seven-band images was individually subjected to iterative clustering to define an optimal control set of no-change pixels, which were selected both by visual inspection of the image and histogram analysis. The addition of Band 4 from the reference image helped ensure that pixels along the full brightness gradient (water, forest, and urban) were selected as candidate control sets. Subsequent iterations of clustering successively eliminated questionable control set pixels until an optimum set was retained. The pixels kept as the no-change control set were then subsampled to produce 666 pixels for each of the water, forest, and urban classes, for a total of 1998 pixels for each subject image. Sorted geographically, half of these pixels were used to develop univariate regression models relating the subject DN to the reference DN for each band; the other 999 pixels were withheld for testing of the normalization models.

Preliminary examination of the data set revealed a wide range of spectral contrasts among land cover types and a generally consistent signature pattern within individual agricultural fields. To reduce the data set size, we elected to use the first three components of the Tasseled Cap transformation (Crist & Cicone, 1984) for further analysis. Previous experience mapping forests in western Oregon demonstrated a great utility in the physical interpretation of the brightness, greenness, and wetness indices for the interpretation of natural conditions (Cohen & Spies, 1992; Cohen et al., 1995; Cohen et al., 1998). The needs of this project afforded us our first opportunity to extend our knowledge of these indices into the agricultural land cover system for which the transformation was originally designed (Kauth & Thomas, 1976).

2.2. Ground and airphoto reference data

Our mapping approach in this project involved stratifying the WRB into four broad cover types: upland forest, urban areas, valley forest, and valley nonforest (agricultural, natural, and built) (Fig. 1). The land cover mapping of the upland forest (defined by a boundary based on the 315-m contour) had already been completed as part of a separate project covering Oregon forests west of the Cascade Range crest (Cohen et al., 2001). The products from that effort were continuous predictions for % green vegetation cover, % conifer cover, and closed conifer stand age, derived from single-date 1988 TM imagery. Thus, our research focused on the other three broad cover types of the basin.

For the urban areas, we obtained six 260-ha 1997 color digital orthophotographs (DOPs) (Table 2) at 1.2-m pixel resolution (Metro; Portland, OR). These photos were used to reference an initial classification of land cover types within the urban areas.

To reference the valley forest, we obtained access to a collection of 1993 color photographs at 1:24,000 scale (WAC; Eugene, OR) (Table 2). These photos were distributed across the valley floor, and we randomly selected 110 photos in forested areas. For 235 forest plots averaging 2 ha in size, we photointerpreted estimates of % cover for conifer, broadleaf, shrub, open, and shadow (Table 2; Fig. 3). Half of these plots were used for training, and the rest were left for testing. In addition to forest, we used the photos to identify 43 plots of semipermanent nonforest (i.e., orchards, vineyards, and silviculture).

The aerial photographs proved adequate for the relatively stable land cover types, but for most agricultural and nonforest classes, annual variation in cropping patterns required time-relevant photography. Thus, our primary reference data were 35-mm color slide photographs [USDA Farm Service Agency (FSA); Tualatin, OR; Table 2]. FSA offices contract annual aerial photography missions to provide documentation of countywide crop conditions to certify farmer's crop reports (Buechel et al., 1989). The FSA agents typically target image collection in late May or early June. Imagery was acquired using standard hand-held 35-mm cameras from a height of approximately 1.5 km. They provide a color image of the land surface that is roughly 3×2 km in size. We purchased 369 slides, covering 33 separate focus areas, from seven different FSA offices. The focus areas were selected both to match the existing 1993 WAC airphoto coverage and to capture the widest diversity of land cover types in each county. Each slide was scanned into a tagged image file (.tif) at 300 dpi using a Polaroid Sprintscan 35/ES slide scanner and then georeferenced to the TM imagery using a minimum of nine ground control points for a root mean square error of under 10 m. To use the slides, we projected them on a white wall above our workstation while displaying the digital mosaic of the scanned and rectified version on the computer monitor. The projected image (about 1:1500) allowed a substantial amount of interpretable detail, with individual trees, houses, roadways, and even plowing patterns and irrigation marks that are easily discernible.

The color and texture of fields on the slides were related to crop types (Goodman, 1964). Most of the field crops, especially grass seed and winter wheat, were at peak growth at the time of image acquisition. The row crops, which were planted later and depend on irrigation through the summer, had barely broken soil and had visual evidence of irrigation. Other land cover types, such as improved pasture and hayfields, were denoted by animal paths or the accumulation of hay bales. We photointerpreted land cover for 501 fields in 5 of the 33 geographically separate focus areas (Fig. 3), and then compared our interpretations with crop reports filed on those fields by the farmers. Only 153 of the 501 fields were included in the crop reporting system for that year (Table 2).

We then used the knowledge gained from the crop reports to develop an interpretation technique, which employed 59 separate land cover codes based on visual interpretation of the FSA slides. In some cases, the land cover code depended on the timing of green-up or senescence, which we inferred from inspection of the five dates of TM imagery. The information obtained from the farmer's crop reports helped us identify several spectrally unique crops (e.g., radish seed, sugar beet seed, and mint). We also created land cover codes for nonagricultural land cover, including rural residential buildings, other urban, wetlands, natural prairies, natural shrub, and oak savanna. Most of these codes were based on our inspection and knowledge of the landscape, without the benefit of verification from the crop reports. Following the verification stage, an additional

Table 2
Ground reference data

Source	Scale/resolution	Date	Used for	Training plots	Testing plots	Total
WAC airphotos	1:24,000	1993	Valley forest	119	116	235
			Nonforest	20	23	43
FSA slides	≈ 1:1500	1992	Verification	153		153
			Nonforest	406	553	959
			Urban		23	23
Metro digital orthophotographs[a]	1.2 m	1997	Urban	–	–	–
Moser landscape photos[a]	n/a	1994–1998	Nonforest	–	–	–
Total				698	715	1413

[a] These data sets were not used to develop training and testing plots but for visual reference and as interpretation aid.

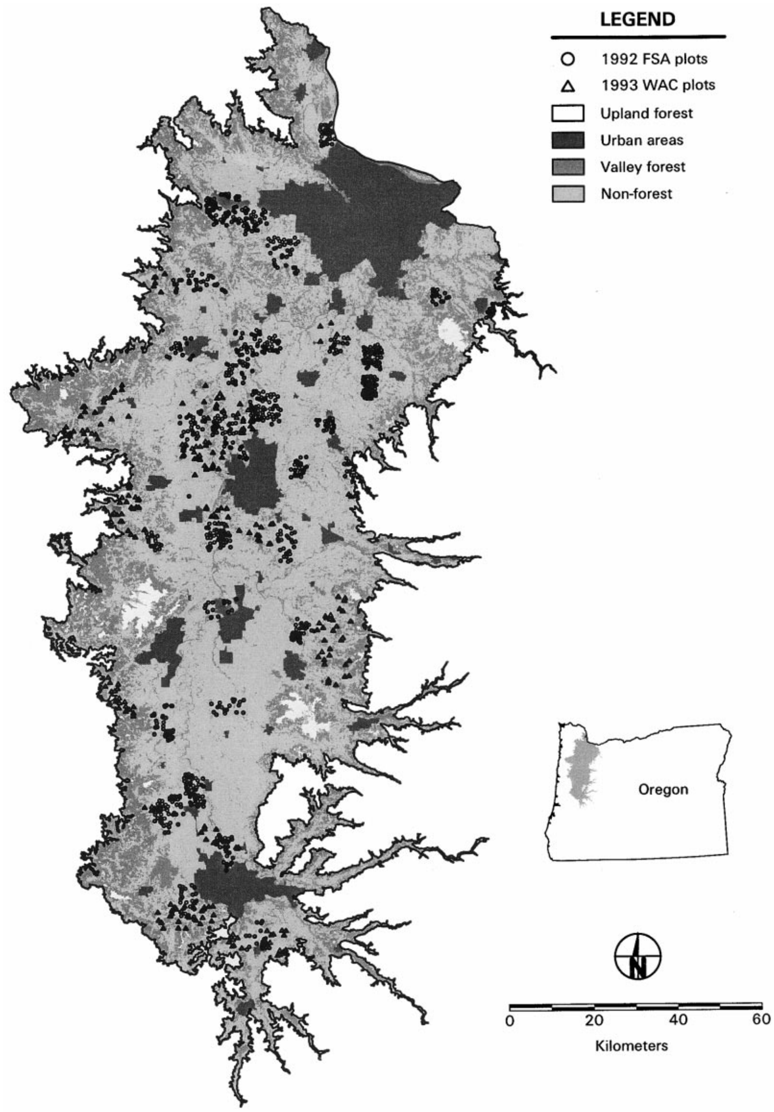

Fig. 3. Ground reference plots (training and testing) for forest and nonforest sites within Willamette Valley, shown over the four mapping units.

634 plots in the remaining 28 focus areas were interpreted to provide a total of 1135 FSA plots for training and testing (Table 2). All of the 153 verification plots were used for training the image classification.

In addition to the photographic data sets, we employed county zoning GIS coverages to help interpret land cover types, as well as a collection of 452 oblique color photographs that were referenced with global positioning satellite-determined points (Tom Moser, personal communication). While these photographs were taken over several years of field reconnaissance after 1992, they were still useful for cross-checking our interpretation of the FSA slides and for identifying general cropping patterns (Fig. 4).

2.3. Image analysis

The hierarchical image processing steps used to construct the WRB land cover map were specifically designed for each of the three broad cover types in this study: urban, valley forest, and nonforest (Ehrlich et al., 1994; Lauver & Whistler, 1993; Pax-Lenney et al., 1996; Fig. 5).

The first step in mapping the Willamette Valley involved stratifying the pixels contained within Oregon's urban growth boundary zoning areas. Each of the 89 urban areas in the WRB (Fig. 1) had an identified boundary. Our goal was to identify several land cover types that could be combined with census data to indicate land use and population density. Unsupervised classification of the 15-band five-date Tasseled Cap data set, using the Metro DOPs as reference, was used to separate urban areas into three desired classes (high-density built, medium-density built, and water), and a confused class (urban other) that was reclustered in later steps.

Secondly, all the pixels outside the urban areas were assessed to distinguish forest vs. nonforest. The forested areas were further classified based on forest characteristics

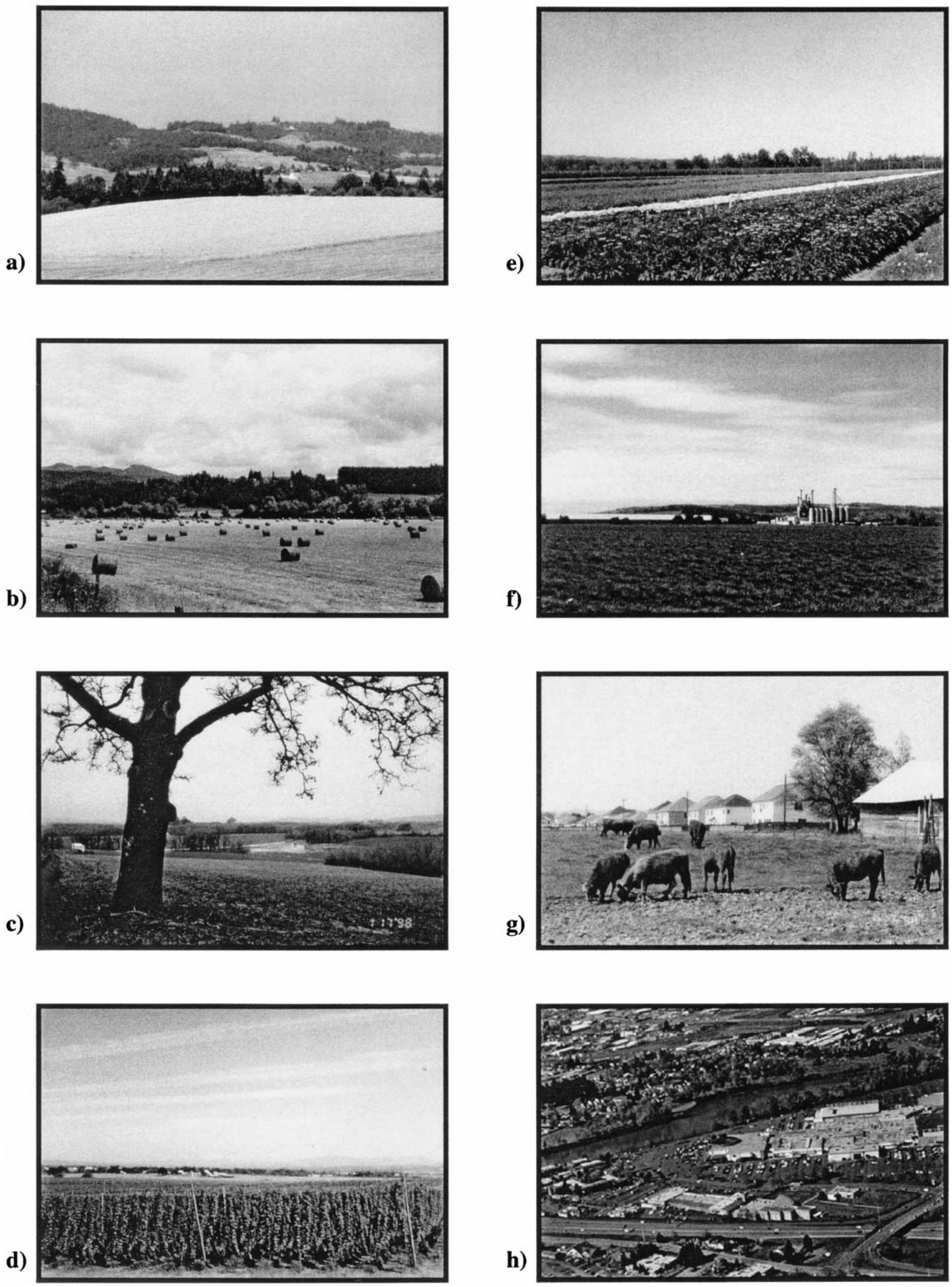

Fig. 4. Photographs that exemplify Willamette Valley landscapes (courtesy of Tom Moser). (a) The bright radish seed crop in the foreground stands out against the mixed forest, pastures, and farm homes of the hills behind. (b) Hayfields typically occupy the vales ringed by broadleaf, and conifer forest stands above. (c) The Willamette Valley contains many creeks that flood during the wet winters, retaining a dense riparian gallery of hardwoods surrounded by grass fields and pastures. (d) Extensive fields of hops, destined for one of Oregon's microbeer productions, line the Willamette River near Salem. (e) The valley's cool dry summers aid several large nursery and container crop operations. (f) The poorly drained southern portion of the valley produces most of the nation's rye grass seed interspersed by farm operations, such as this poultry farm. (g) Farms and fields are giving way to suburban expansion throughout the valley, but especially in the high-growth region around Portland. (h) Valley River mall in Eugene, next to the Willamette River, represents a high-density built environment typical of the more populous urban areas.

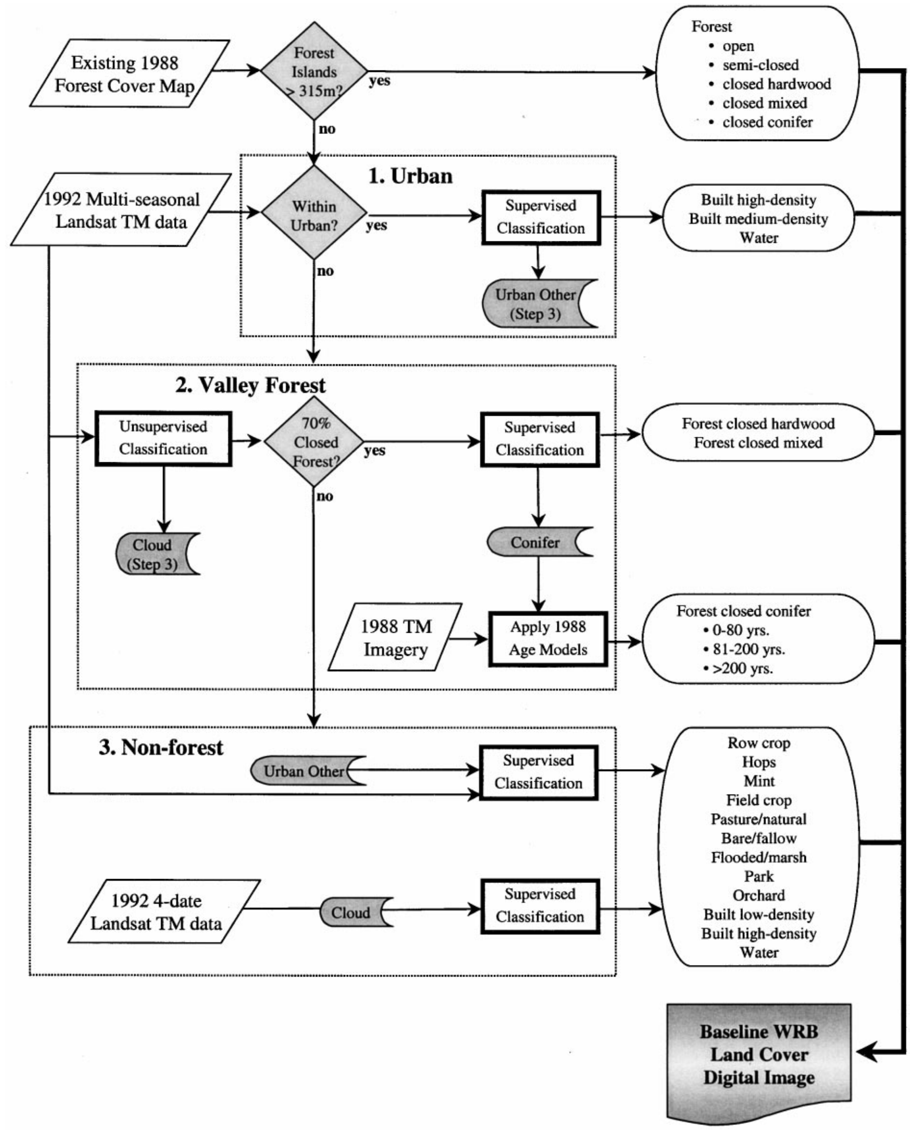

Fig. 5. Flow chart of the image processing steps.

(Fig. 5). The training plots developed from the 1993 color photographs were used to label unsupervised clusters derived from the 15-band Tasseled Cap data. Pixels labeled as closed forest (defined as $\geq 70\%$ forest cover) were separated into closed conifer (0–30% hardwood), closed mixed (31–69% hardwood), and closed hardwood (70–100% hardwood) classes with a supervised classification (Schriever & Congalton, 1995). Closed conifer pixels were then reclassified into three age categories by applying multiple regression stand age models developed for the upland forest (Cohen et al., 2001) to the 1988 TM imagery for which they were developed.

The third step involved classification of all remaining pixels, including the urban other class from the first step and the pixels rejected as closed forest from the second step (Fig. 5). We had some confidence in the spectral separability of tentative class groups based on preliminary graphs of the training clusters (Fig. 6). The temporal signatures of the agricultural cover types (Lo et al., 1986; Williams et al., 1987), especially the Tasseled Cap greenness component, resembled a Willamette Valley cropping calendar (ODA, 1999). Using a 16-band image created by adding a DEM to the 15-band Tasseled Cap spectral data set, we conducted a maximum likelihood supervised classification to produce 10 major classes (tree crop, row crops, field crops, pasture, natural, bare, built, seasonally flooded, irrigated, and water). We separated the major groups into subclasses, where further divisions were statistically justifiable (San Miguel-Ayanz & Biging, 1997).

One final clustering was performed to reclassify pixels that were obscured by clouds in the June 7 image (Fig. 5). This was done with a supervised classification of a 13-band (four-date with DEM) image to cluster those pixels into the final classes using similar decision rules as above.

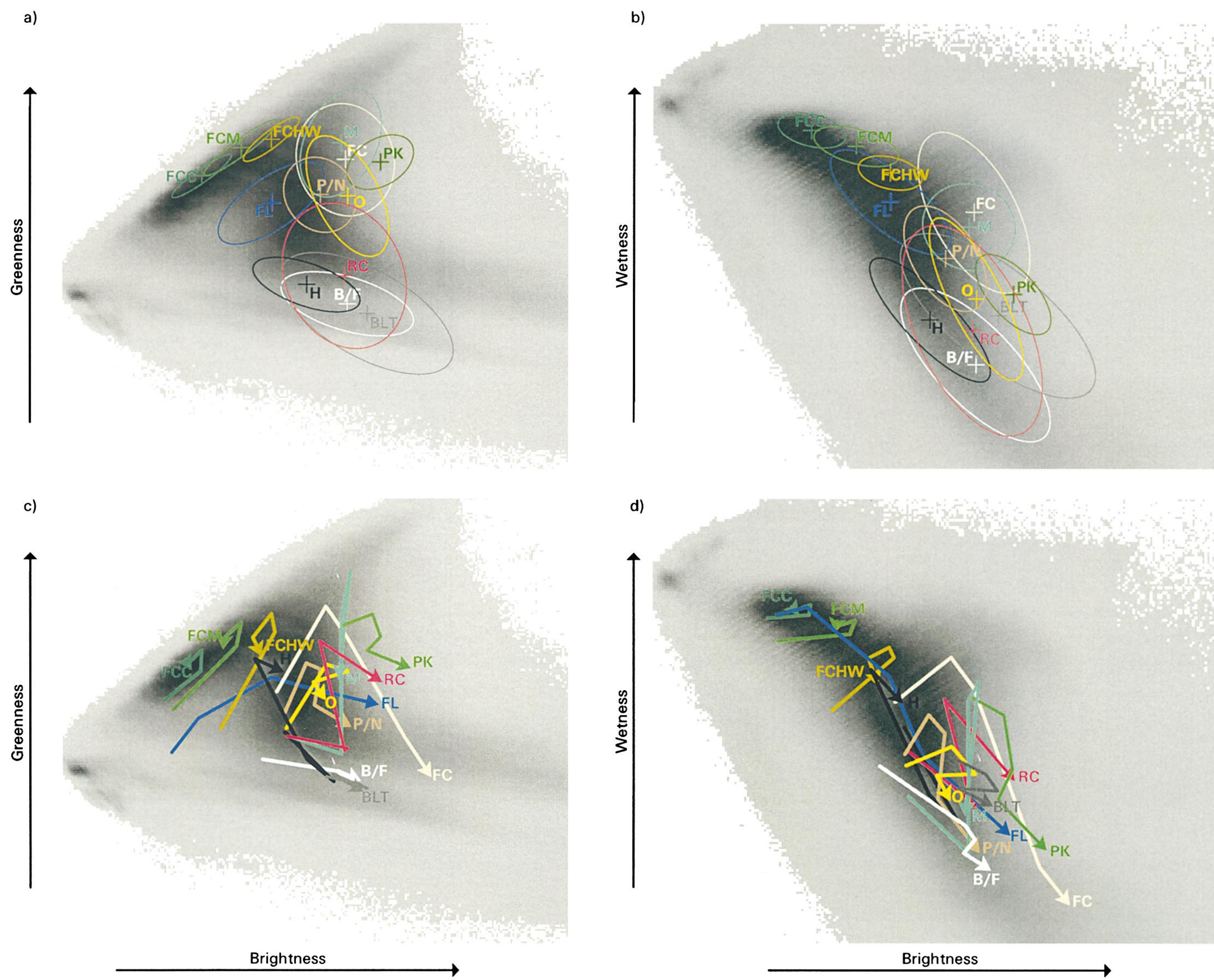

Fig. 6. Spectral signature mean with ellipses drawn at one standard deviation for training plots in (a) B-G and (b) B-W feature spaces for 13 valley land cover types for the 7 June image. Spectral signature mean trajectories for the same training plots for the five image dates in (c) B-G and (d) B-W feature space. The arrows for each land cover type show the change in the mean values of the training plots from March through August. See Table 6 for code definitions.

Table 3
Radiometric normalization models

Source image date	Band normalization equations	Model R^2	Testing R^2	Testing slope	Testing intercept
March 19	b1n = 1.436*b1 − 20.535	.889	.896	1.02	− 1.47
	b2n = 1.463*b2 − 6.449	.887	.894	1.01	− 0.31
	b3n = 1.635*b3 − 11.869	.919	.924	1.01	− 0.23
	b4n = 1.449*b4 − 3.738	.922	.920	0.99	0.46
	b5n = 1.412*b5 − 0.661	.933	.933	1.00	0.30
	b7n = 1.567*b7 − 0.911	.931	.935	1.02	− 0.14
May 6	b1n = 1.151*b1 − 9.082	.964	.955	0.98	2.15
	b2n = 1.136*b2 − 2.215	.968	.956	0.98	1.27
	b3n = 1.193*b3 − 2.615	.972	.965	1.00	0.46
	b4n = 1.059*b4 + 0.697	.955	.949	0.99	0.91
	b5n = 1.117*b5 − 0.655	.987	.984	1.00	0.60
	b7n = 1.121*b7 + 0.320	.975	.975	0.99	0.73
July 25	b1n = 0.832*b1 + 16.497	.897	.892	1.00	− 0.13
	b2n = 0.853*b2 + 6.057	.822	.816	0.96	1.00
	b3n = 0.844*b3 + 6.100	.824	.805	0.93	1.57
	b4n = 1.011*b4 + 4.597	.945	.941	1.01	− 0.28
	b5n = 1.037*b5 + 2.750	.936	.914	0.99	0.09
	b7n = 0.976*b7 + 1.423	.846	.829	1.00	− 0.17
August 26	b1n = 1.114*b1 + 7.161	.913	.902	0.99	0.67
	b2n = 1.056*b2 + 5.376	.788	.772	1.03	− 0.67
	b3n = 1.017*b3 + 7.049	.777	.684	0.93	1.69
	b4n = 1.139*b4 + 8.358	.969	.966	1.00	0.13
	b5n = 1.178*b5 + 2.639	.955	.949	0.98	0.76
	b7n = 1.206*b7 + 2.070	.895	.886	1.00	0.16

The band normalization equations calculate the normalized band value (b*x*n) as a function of the raw value (b*x*), where x is the band number. Model R^2 was calculated for the training pixels, while testing R^2 was calculated on an independent testing set. The testing slope and testing intercept refer to the regression line of predicted vs. observed values for the testing set. Testing slopes close to 1 and testing intercepts close to 0 are considered ideal.

2.4. Map generation and error characterization

For the generation of our final map, we combined the output classes from the three stages of image processing to produce 20 distinct classes. The accuracy of the entire map was assessed by constructing an error matrix using 715 testing plots divided among valley forest, nonforest, and urban (Table 2). Assessment of the closed forest conifer age classes was done separately using ground reference data for 71 plots in the upland forest area (Cohen et al., 2001). For the land cover class accuracy assessment, we employed a mode-decision rule for each plot determination (i.e., the predicted value of a plot was set to the class that had the highest number of pixels within that plot; there were no ties).

3. Results

Radiometric normalization coefficients of determination for the models ranged from 0.78 to 0.99 (Table 3). Slopes

Table 4
Preliminary FSA slide photointerpretation error matrix

	FSA crop report reference														
Photo interpretation	BER	CO	ERC	F	FC	G	IFC	LFC	M	O	P	R	RC	X	Total
Berries (BER)	1														1
Conifer orchard (CO)		1													1
Early row crop (ERC)			1									1			2
Fallow (F)				3		1		1					1		6
Field crop (FC)					40	4		2			1				47
Grass seed (G)						26									26
Irrigated field crop (IFC)				1			4								5
Late field crop (LFC)								2			1				3
Mint (M)									3						3
Orchard (O)										8					8
Pasture (P)				1	1	1					16				19
Radish seed (R)												3			3
Row crop (RC)					1		1						25		27
Christmas trees (X)														2	2
Total	1	1	1	5	42	32	5	5	3	8	18	4	26	2	153
Accuracy (%)	100	100	100	60	95	81	80	40	100	100	89	75	96	100	88.2

and offsets varied from 0.83 to 1.64 and from -21 to 16, respectively. The testing half of the control set was used to determine the effectiveness of the normalization equations. For each image and every band, the slope of the line between the normalized subject and reference pixels was close to 1 and the intercept was close to 0, indicating that the regression equations were effective at normalizing the imagery.

Initial FSA interpretations within 5 of the 33 study sites were confirmed for 153 plots. Only 18 plots were interpreted incorrectly, for an overall photointerpretation error of 12% (Table 4).

While most of the upland forest was intentionally excluded from this study, several small islands of land (totaling 257 km^2) above 315-m elevation were contained within the study boundary. These islands represented only 1.9% of the study area and were mapped into seven forest classes: open (<31% green vegetation cover, 3.8%), semi-closed (31–69% green vegetation cover, 10.2%), closed hardwood (7.8%), closed mixed (36.2%), closed conifer 0–80 years (22.4%), closed conifer 81–200 years (16.7%), and closed conifer >200 years (2.9%). The rest of the study area was mapped in three successive stages as urban areas (13.0%), valley forest (26.3%), and nonforest (58.8%).

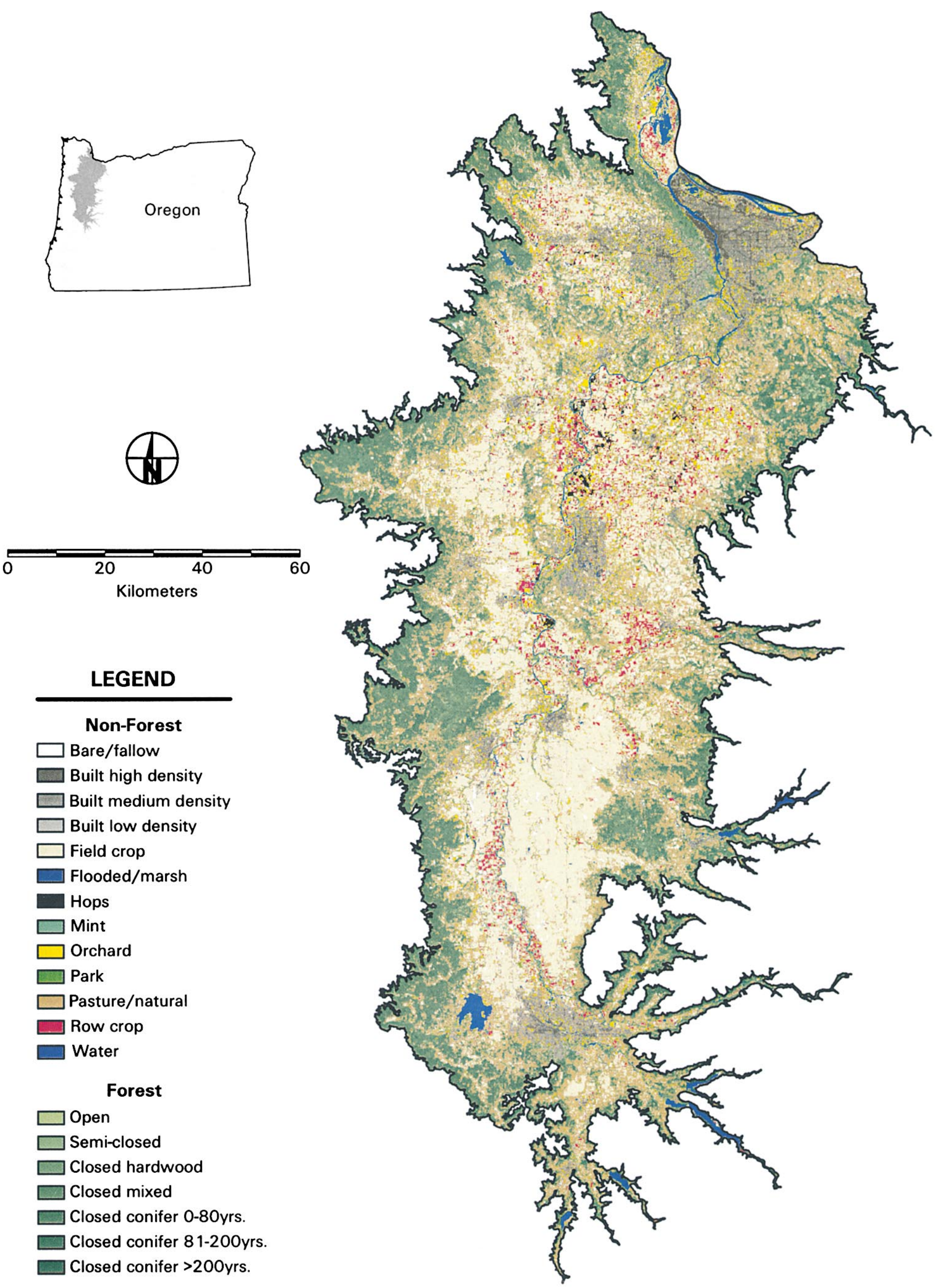

Fig. 7. The 1992 20-class land cover map of the Willamette Valley.

Table 5
Final land cover classes for WRB study area

Class	Area (km^2)	%
Bare/fallow	276.9	2.0
Built high-density	228.4	1.7
Built low-density	315.3	2.3
Built medium-density	642.0	4.6
Field crop	3233.8	23.4
Flooded/marsh	88.6	0.6
Forest closed conifer 0–80 years	872.2	6.3
Forest closed conifer 81–200 years	743.9	5.4
Forest closed conifer >200 years	170.9	1.2
Forest closed hardwood	1046.8	7.6
Forest closed mixed	1727.9	12.5
Forest open	9.7	0.1
Forest semiclosed	26.2	0.2
Hops	33.0	0.2
Mint	28.7	0.2
Orchard	460.6	3.3
Park	92.2	0.7
Pasture/natural	3032.7	21.9
Row crop	570.5	4.1
Water	226.0	1.6
Total	13,826.3	100.0

Most of the 1802-km^2 urban area was mapped into three built classes using a subjective standard for the level of development: built high-density (10.3%), built medium-density (35.6%), and built low-density (4.5%). The remainder of the urban area was mapped as pasture/natural (14.1%), field crop (9.6%), orchard (7.3%), forest closed hardwood (7.1%), forest closed mixed (4.6%), and water (2.1%). Nine other classes combined to account for less than 5% of the area.

We labeled 3642 km^2 of the study area as valley forest, defined as forest with at least 70% canopy closure, and further distinguished this cover type into five classes based on the estimated percentages of hardwood and conifer (Cohen et al., 2000): closed hardwood (22.1%), closed mixed (37.6%), closed conifer 0–80 years (20.0%), closed conifer 81–200 years (16.8%), and closed conifer >200 years (3.4%).

In the remaining 8127 km^2 of nonforested area, we mapped the landscape into 17 land cover classes, including a small percentage of forest classes (5.7%), which were obtained by reexamining the pixels rejected as forest in the second classification step. The majority of this area was mapped as field crop (37.7%) or pasture/natural (34.2%), two land cover types that are prevalent in the valley. Other important land cover classes included row crop (6.7%), orchard (4.1%), bare/fallow (3.3%), built low-density (2.9%), and water (2.3%). The 28 km^2 of pixels covered with cloud and cloud shadow were then classified into the same land cover types using a cloud-free training set.

The final map was created by combining the three stages of this study with the existing upland forest map (Fig. 5) to generate a 20-class map of the study area (Fig. 7). These classes are presented in Table 5, which reveals that the most dominant land cover types in the valley are field crop (23.4%), pasture/natural (21.9%), and forest closed mixed (12.5%). The error matrix for the map (Table 6), excluding

Table 7
Closed conifer forest age error matrix

	Reference				Accuracy
Map prediction	1–80 years	81–200 years	>200 years	Total	(%)
1–80 years	15	4		19	78.9
81–200 years	5	20	2	27	74.1
>200 years		5	20	25	80.0
Total	20	29	22	71	
Accuracy (%)	75.0	69.0	90.9		77.5

Table 6
Error matrix for land cover (excluding conifer age) using the mode-decision rule to assign map classes to each polygon

	Reference																	Accuracy
Map prediction	B/F	BHD	BLD	BMD	FC	FL	FCC	FCHW	FCM	H	M	O	PK	P/N	RC	W	Total	(%)
Bare/fallow (B/F)	21	1			1							2		1	3		29	72.4
Built high-density (BHD)		9	1												1		11	81.8
Built low-density (BLD)		3	6											2			11	54.5
Built medium-density (BMD)			3	10										2			15	66.7
Field crop (FC)					175	3					3	4	1	17	17		220	79.5
Flooded/marsh (FL)						4											4	100.0
Forest closed conifer (FCC)							44		11					4			59	74.6
Forest closed hardwood (FCHW)								31	1			4		1			37	83.8
Forest closed mixed (FCM)							3	12	16					2			33	48.5
Forest semiclosed					1									2			3	0.0
Hops (H)										17				1	2		20	85.0
Mint (M)					3						10				2		15	66.7
Orchard (O)	2				1							32		6		1	42	76.2
Park (PK)					1							1	2	1			5	40.0
Pasture/natural (P/N)	1		8		17		1	1		3		11		73	3		118	61.9
Row crop (RC)	1				13					1					77		92	83.7
Water (W)																1	1	100.0
Total	25	13	18	10	212	7	48	44	28	21	13	54	3	112	105	2	715	
Accuracy (%)	84.0	69.2	33.3	100.0	82.5	57.1	91.7	70.5	57.1	81.0	76.9	59.3	66.7	65.2	73.3	50.0		73.8

the closed conifer age classes, indicates an overall map accuracy of 73.8%. The accuracy assessment for the closed conifer forest age classes was performed independently, using ground reference sample points from the upland forest region (Cohen et al., 2001). Table 7 shows a closed conifer forest age accuracy of 77.5%.

The final 20-class Willamette Valley land cover map portrays a landscape in which land use is determined by topography, access to irrigation, and urbanization. Most of the built pixels are found within the major urban centers of Portland, Salem, and Eugene (Figs. 1 and 7). In the flat southern portion of the valley characterized by deep silty soils, the predominant land cover is field crop, exemplified best by rye grass grown for seed. In the vicinity of the Willamette River and its major tributaries, the availability of surface water for irrigation makes row crop farming feasible, as well as other lucrative crops, such as mint, hops, and orchards. The greatest diversity of crop types is found north of Salem and outside Portland, where farm tracts are smaller and more varied than in the south. Where foothills break the valley floor, the pasture/natural class dominates. This class includes pastures, shrub lands, oak savanna, vineyards, and Christmas tree plantations. Along the fringe of the valley toward the Coast Ranges and the Cascades, pasture/natural cover gives way to closed forest, including vast oak and conifer stands.

4. Discussion

4.1. Desired vs. mapped classes

The main objective of this project was to deliver a map of the Willamette Valley that matched a list of desired land use and land cover classes (Table 1). Many of those classes, especially in the urban, built, and hydro groups, were essentially land use designations that "convey the human employment of the land," as opposed to land cover classifications that "denote the physical state of the land" (Turner & Meyer, 1994). We knew at the onset that we would be unable to map certain land use classes with TM imagery, but that many of those classes could be mapped with ancillary GIS data, such as census data, zoning information, and transportation coverages. Therefore, we were more concerned with detecting spatial variation within the forested, agriculture, and open/woody classes.

For both the forested and the nonforested portions of the valley, we collected ground reference data that reflected both the desired class list, as well as the full landscape diversity of the valley. The combination of a rich ground reference data set (Table 2) with an extensive nonforest cover scheme allowed us to finely separate the TM imagery into unique land cover classes. To isolate the forested portion of the valley, we generated percent forest cover data for 235 photointerpreted plots similar to the methods of Cohen et al. (2001). In the nonforest, we used a combination of the FSA slides and the multidate Tasseled Cap images to identify 59 unique types of agricultural and natural land cover distributed over a wide geographic range (Fig. 3). Our photointerpretation of the more common land cover classes was independently verified by FSA crop reports (Table 4). Having confidence in our photointerpretation, combined with the broad diversity and areal representation of the ground reference data set, gave us a considerable advantage in using a supervised classification to separate the nonforest pixels into the final classes (Table 5).

The rich five-date TM data set allowed us to map many classes that could not have been captured without multiseasonal imagery (Lo et al., 1986; Williams et al., 1987). A different map of the basin (Uhrich & Wentz, 1999), which used June and August 1992 images for the WRB, mapped nine land cover classes (urban, water, mature forest, regrowth forest, nonforest upland, native vegetation-valley floor, irrigated crops, grass fields/small grains, and perennial snow). The addition of three more dates allowed us to separate the nonforested portion of the valley into nine classes other than water and built. For example, the bare fallow class was discernable, because we knew that throughout that growing season, there was no green vegetation cover on those fields. Likewise, the flooded/marsh class required having imagery from the wet season (March), as well as throughout the rest of the growing season to differentiate seasonal wetlands from permanent water bodies.

Not surprisingly, the spectral separability of the TM imagery did not match the highly refined ground reference data set, and we were unable to capture the full complement of known land cover types in the valley (Table 8). Many of our initial classification results were later aggregated into broader classes (e.g., pasture, natural grasslands, natural shrub, and Christmas trees were combined to form one pasture/natural class). Other spectrally distinct classes were collapsed into final classes either because they represented very small percentages of the valley (e.g., sugar beet seed) or because we lacked sufficient ground reference plots to statistically justify separate classes (e.g., closed oak forest). In addition, we were not able to map new crops, such as hybrid poplar and meadowfoam, which have just recently appeared on the landscape in sufficient area to warrant mapping.

Our attempt to estimate percent impervious cover within urban areas was confounded by a lack of usable ground reference data (Plunk et al., 1990). However, for our final classes, we decided to create three relative levels of built land cover types (built high-density, built medium-density, and built low-density) that would reflect the relationship between vegetation and impervious cover. The high-density class mapped large buildings, parking lots, and other artificial features with minimal vegetative cover; the medium-density class reflected apartment buildings and residential settings where vegetation was present but not prevalent; and the low-density class represented the well-vegetated suburbs

Table 8
Final map status of the classes desired by the PNW-ERC (n/m = not mapped)

Desired class	Final map class	Comments
1. Urban		
a. Residential	n/m	Land use classification
b. Commercial	n/m	Land use classification
c. Industrial	n/m	Land use classification
d. Open space	Park, pasture/natural	
e. Herbaceous-roads	n/m	Spatial resolution limitations
2. Built (nonurban)		
a. Commercial	n/m	Land use classification
b. RR2-5 zoning	n/m	Land use classification
c. Within 2 acres of structures	n/m	Land use classification
d. Railroad	n/m	Spatial resolution limitations
e. Roads	n/m	Spatial resolution limitations
f. Revetments	n/m	Spatial resolution limitations
3. Hydro		
a. Headwater streams	n/m	Spatial resolution limitations
b. Open-standing water	Water	
c. Streams > first order	Water, n/m	Spatial resolution limitations
4. Forested		
a. 0–40-year-old Douglas fir	Forest closed conifer 0–80 years	Derived from continuous age estimates
b. 41–120-year-old Douglas fir	Forest closed conifer 0–80 years, forest closed conifer 81–200 years	Derived from continuous age estimates
c. >120-year-old Douglas fir	Forest closed conifer 81–200 years, forest closed conifer > 200 years	Derived from continuous age estimates
d. Mixed conifer/deciduous	Forest closed mixed	
e. Deciduous	Forest closed hardwood	
f. Lower riparian forest	Forest closed mixed, forest closed hardwood	Proximity to water was not mapped
5. Agriculture		
Grass seed/grain	Field crop	
Hybrid poplar	n/m	Inadequate ground reference
Nursery operations	n/m	Spectral resolution limitations
Orchards	Orchard	
Pasture and haylands	Pasture/natural	
Row crops	Row crop	
Vineyards, berries, and hops	Row crop, pasture/natural, hops	
Christmas trees	Pasture/natural	
Mint	Mint	
Meadowfoam	n/m	Inadequate ground reference
Confined animal operations	n/m	Inadequate ground reference
Farmsteads	Built low-density	
6. Open/woody		
Shrub/brush	Pasture/natural	
Fence rows	n/m	Spatial resolution limitations
Oak savanna	n/m	Spectral resolution limitations
Prairie (grass/forb)	Pasture/natural	
Marsh (nontreed wetlands)	Flooded/marsh	
7. Percent Impervious surface		
< 10%	n/m	Reflected by built low-density
10–20%	n/m	Reflected by built medium-density
>20	n/m	Reflected by built high-density

where trees, shrubs, and lawns share the spectral signal more equally with roads and rooftops. As there was no available ground reference data, we could not ascertain how well these class distinctions modeled percent impervious cover. Furthermore, our mapping of the urban areas may have been limited due to our exclusion of the fourth Tasseled Cap band (Goward & Wharton, 1984).

4.2. Multiseasonal Tasseled Cap trajectories

A second objective of our research was to extend our working knowledge of the Tasseled Cap transformation into the agricultural lowlands of the WRB. We had previously relied on ancillary GIS data to separate forest (especially hardwood) and agricultural cover in the valley (Cohen et al., 2001), but for this project, we attempted to use the spectral data alone to guide the separation of forest, agricultural, and natural land cover types. In addition to conserving storage space, the TM Tasseled Cap transformation produces indices that have physically interpretable characteristics, both in geographic space and in feature space (Crist & Cicone, 1984; Crist, Laurin, & Cicone, 1986; Kauth & Thomas, 1976). The more familiar spectral responses of forest and shrub cover were easily distinguishable against a backdrop of spectrally unique agricultural crops. In feature space, the multiseasonal trajectories of our training plot means were well separated in brightness-greenness (B-G) and brightness-wetness (B-W) space (Fig. 6c and d).

A major advantage of using multiseasonal Tasseled Cap imagery is the ability to separate land cover classes with attention to the seasonal greenness curves (Crist & Malila, 1980; Lo et al., 1986). Fig. 6a shows the confusion in B-G space that would occur by using only one date of imagery (in this case, 7 June) for a supervised classification. While the forest and flooded/marsh classes may have been separable in this instance, the remaining classes appear confused in two major clusters depending on the presence or absence of vegetative cover in June. For that one date, the row crop, hops, and bare/fallow classes are indistinguishable, since all those plots reflected bare soils at that time. Similarly, the agricultural cover types that were vegetated in June (field crop, mint, and orchard) are confused with each other, and at the same time, they are closely associated with pasture/natural and park cover responses.

The five-date multiseasonal TM data set facilitated better separation of land cover classes by allowing classification of the pixels based on their temporal trajectories through the growing season. In feature space, these trajectories can be plotted as vectors moving through time (Fig. 6c and d). Each training reference mean is more significantly separable, because it defines that cover type in 15 dimensions through time rather than just in the three dimensions of a one-date Tasseled Cap image. The flooded/marsh class, for example, begins its path through B-G space near the water bulb (low brightness, low greenness) in March, and then increases dramatically in brightness through the growing season, as the surface water and soil moisture diminish. Row crop and field crop classes are readily separable, as field crops begin the growing season with high-greenness peak in May and drop rapidly as natural precipitation diminishes during the dry months of July and August, whereas, row crops are planted later and do not green up until July. Parklands remain high in greenness throughout the growing season with the aid of irrigation and maintenance. At the other end of the spectrum, the bare/fallow class has low greenness throughout the season and increases in brightness as the bare soil loses moisture, which is evidenced by a steep decline in wetness (Crist, Laurin, Colwell, & Kauth, 1984). While the mint and hops signals are separable based on the timing and direction of their feature space trajectories, the orchard and pasture/natural classes show a considerable amount of overlap in both B-G and B-W space. It is interesting to note the behavior of the orchard signal, which resembles that of the forest closed hardwood class but with higher brightness and lower wetness. We speculate that these differences are caused by the ground cover between orchard trees. Many of the orchards we sampled were young filbert orchards with considerable gaps between trees. These gaps typically reveal grass or bare soil, which directs the orchard response away from that of forest closed hardwood. The three broad forest classes are well separated, both in the leaf-off condition in March and by the movement of the hardwood and mixed classes from more open to their closed canopy positions in both feature spaces.

The position and direction of the training class mean trajectories correlate well with the discoveries of Crist et al., 1986, who analyzed the first four bands of the Tasseled Cap transformation using both laboratory and field information. With the exceptions noted above, we observed similar feature space trajectories through the growing season. For the late-season cover types (row crop, hops, and mint), the movement from March to May was marked by sharp decrease in wetness and an increase in brightness, as the bare soil dried before the growing season began. The physical interpretations of brightness, greenness, and wetness allowed us to infer a great deal of information about the vegetative cover of our study area at each of our acquisition dates.

4.3. Summary

Our purpose in this project was to produce a land cover map that would serve the needs of the PNW-ERC in their goal of characterizing the existing conditions of the WRB, both as a baseline for later research and as the starting point for the development of futures scenarios (PNW-ERC, 2000). We produced a map with 20 urban, agricultural, and natural land cover classes.

Since our work was based almost solely on predicting land cover from TM imagery, the first task of the consortium was to augment our map with available ancillary data, especially US Census data, transportation information, and hydrology coverages. In addition, the map was amended using an agricultural projection model that employed current knowledge of irrigation withdrawal permits and county cropping statistics to predict spatial agricultural patterns for a given year. The resultant map (Existing Conditions 1990) features 60 classes, representing a wide variety of urban, forest, and nonforest land use and land cover types (PNW-ERC, 2000).

The major strengths of our mapping approach came from the wealth of interpretable spectral information available in our multiseasonal Tasseled Cap imagery, especially when trained using the FSA crop compliance photography. While several TM-based vegetative indices and band ratios have been applied to land cover mapping (Lauver & Whistler, 1993; Lo et al., 1986; Pax-Lenney et al., 1996; Williams et al., 1987), we must conclude from our experience that a land cover mapping project such as this, across a large region with many diverse land cover types, could be accomplished with the analysis of multiseasonal Tasseled Cap imagery (Crist, 1984). We feel confident that our map product serves the needs of the consortium and other regional users, however, we hope to improve upon this effort in the future, perhaps by incorporating real-time ground reference data collection with the increased data availability provided by Landsat 7 and other sensors.

Acknowledgments

The authors would like to acknowledge the support of the EPA and Oregon State University for funding this research (cooperative agreement no. CR824682), especially the dedicated direction of project leader Joan Baker and principal investigators Stan Gregory, David Hulse, and Rick Edwards. Although the research described in this article has been funded (wholly or in part) by the US EPA, it has not been subjected to the Agency's review and therefore does not necessarily reflect the views of the Agency, and no official endorsement should be inferred. Mike Shuft, Tom Moser, Daryl Ehrensing, Michelle Ham, and Patti Anderson contributed greatly to our construction of an accurate and comprehensive ground reference database, either through their suggestions for photointerpretation technique or by sharing their vast knowledge of Willamette Valley agricultural landscapes. Additionally, we greatly appreciate the editorial comments from Sara Lipow, Ross Lunetta, and other reviewers.

References

Adinarayana, J., Flach, J. D., & Collins, W. G. (1994). Mapping land use patterns in a river catchment using geographical information systems. *Journal of Environmental Management*, *42*, 55–61.

Bauer, M. E., Hixson, M. M., Davis, B. J., & Etheridge, J. B. (1978). Area estimation of crops by digital analysis of Landsat data. *Photogrammetric Engineering and Remote Sensing*, *44*, 1033–1043.

Brewster, C. C., Allen, J. C., & Kopp, D. D. (1999). IPM from space: using satellite imagery to construct regional crop maps for studying crop–insect interaction. *American Entomologist*, *45*, 105–117.

Brisco, B., & Brown, R. J. (1995). Multidate SAR/TM synergism for crop classification in western Canada. *Photogrammetric Engineering and Remote Sensing*, *61*, 1009–1014.

Buechel, S. W., Philipson, W. R., & Philpot, W. D. (1989). The effects of a complex environment on crop separability with Landsat TM. *Remote Sensing of Environment*, *27*, 261–272.

Carbone, G. J., Narumalani, S., & King, M. (1996). Application of remote sensing and GIS technologies with physiological crop models. *Photogrammetric Engineering and Remote Sensing*, *62*, 171–179.

Cohen, W. B., & Fiorella, M. (1998). Comparison of methods for detecting conifer forest change with Thematic Mapper imagery. In: R. S. Lunetta & C. D. Elvidge (Eds.), *Remote sensing change detection: environmental monitoring methods and applications* (pp. 89–102). Chelsea, Michigan: Ann Arbor Press.

Cohen, W. B., Fiorella, M., Gray, J., Helmer, E., & Anderson, K. (1998). An efficient and accurate method for mapping forest clearcuts in the Pacific Northwest using Landsat imagery. *Photogrammetric Engineering and Remote Sensing*, *64*, 293–300.

Cohen, W. B., Maiersperger, T. K., Spies, T. A., & Oetter, D. R. (2001). Modeling forest cover attributes as continuous variables in a regional context with Thematic Mapper data. *International Journal of Remote Sensing* (in press).

Cohen, W. B., & Spies, T. A. (1992). Estimating structural attributes of Douglas fir/western hemlock forest stands from Landsat and SPOT imagery. *Remote Sensing of Environment*, *41*, 1–17.

Cohen, W. B., Spies, T. A., & Fiorella, M. (1995). Estimating the age and structure of forests in a multi-ownership landscape of western Oregon, U.S.A. *International Journal of Remote Sensing*, *16*, 721–746.

Coppin, P. R., & Bauer, M. E. (1996). Digital change detection in forest ecosystems with remote sensing imagery. *Remote Sensing Reviews*, *13* (3–4), 207–234.

Crist, E. P. (1984). Effects of cultural and environmental factors on corn and soybean spectral development patterns. *Remote Sensing of Environment*, *14*, 3–13.

Crist, E. P., & Cicone, R. C. (1984). A physically-based transformation of Thematic Mapper data — the TM Tasseled Cap. *IEEE Transactions on Geosciences and Remote Sensing*, *GE-22*, 256–263.

Crist, E. P., Laurin, R., & Cicone, R. C. (1986). Vegetation and soils information contained in transformed Thematic Mapper data. *Proceedings of IGARSS '86 symposium, Zurich, 8–11 Sept.* (pp. 1465–1470) Noordwijk: ESA Publication Div.

Crist, E. P., Laurin, R., Colwell, J. E., & Kauth, R. J. (1984). *Investigations of vegetation and soils information contained in Landsat Thematic Mapper and multispectral scanner data (final report 160366-101-F)*. Ann Arbor, MI: Environmental Research Institute of Michigan (107 pp.).

Crist, E. P., & Malila, W. A. (1980). A temporal-spectral analysis technique for vegetation applications of Landsat. In: *Proceedings of the 14th international symposium on remote sensing of environment, San Jose, Costa Rica* (pp. 1031–1040) Ann Arbor: Environmental Research Institute of Michigan.

Eckhardt, D. W., & Verdin, J. P. (1990). Automated update of an irrigated lands GIS using SPOT HRV imagery. *Photogrammetric Engineering and Remote Sensing*, *56*, 1515–1522.

Ehrlich, D., Estes, J. E., Scepan, J., & McGwire, K. C. (1994). Crop area monitoring with an advanced agricultural information system. *Geocarto International*, *9*, 31–42.

Environmental Protection Agency [EPA]. (1997). Western Ecology Division, National Health and Environmental Effects Research Laboratory, Pacific Northwest Research Program, May 1997 Peer Review, Corvallis, OR.

Franklin, J. F., & Dyrness, C. T. (1988). *Natural vegetation of Oregon and Washington*. Corvallis, OR: Oregon State Univ. Press (452 pp.).

Goodman, M. S. (1964). Criteria for the identification of types of farming on aerial photographs. *Photogrammetric Engineering*, *30*, 984–990.

Goward, S. N., & Wharton, S. W. (1984). Use of the TM Tasseled Cap transform for interpretation of spectral contrasts in an urban scene. *Proceedings of the symposium on machine processing of remotely sensed data, Purdue University, West Lafayette, IN, 12–14 June* (pp. 84–88) West Lafayette, IN: Purdue Research Foundation.

Haack, B., Bryant, N., & Adams, S. (1987). An assessment of Landsat MSS and TM data for urban and near-urban land-cover digital classification. *Remote Sensing of Environment*, *21*, 201–213.

Henebry, G. M. (1993). Detecting change in grasslands using measures of spatial dependence with Landsat TM data. *Remote Sensing of Environment*, *46*, 223–234.

Hewitt, M. J. III (1990). Synoptic inventory of riparian ecosystems. *Forest Ecology and Management*, *33/34*, 605–620.

Hulse, D., Flaxman, M., Richey, D., Goorjian, L., Diethelm, D., Freemark, K., White, D., Hummon, C., Eilers, J., Bernert, J., & Radosevich, S. (1999). *Possible futures for the Muddy Creek Watershed,* *Benton County, Oregon*. Available at: http://ise.uoregon.edu/Muddy/Muddy_abstract.html.

Jackson, P. L., & Kimerling, A. J. (1993). *Atlas of the Pacific Northwest*. Corvallis, OR: Oregon State Univ. Press (152 pp.).

Johannsen, C. L., Davenport, W. A., Millet, A., & McWilliams, S. (1970). The vegetation of the Willamette Valley. *Annals of the Association of American Geographers*, *61*, 286–302.

Kauth, R. J., & Thomas, G. S. (1976). The Tasseled Cap — a graphic description of the spectra-temporal development of agricultural crops as seen by Landsat. *Proceedings of the symposium on machine processing of remotely sensed data, Purdue University, West Lafayette, IN, 6 June–2 July* (pp. 41–51) New York: Institute of Electrical and Electronics Engineers.

Lauver, C. L., & Whistler, J. L. (1993). A hierarchical classification of Landsat TM imagery to identify natural grassland areas and rare species habitat. *Photogrammetric Engineering and Remote Sensing*, *59*, 627–634.

Lo, T. H. C., Scarpace, F. L., & Lillesand, T. M. (1986). Use of multitemporal spectral profiles in agricultural land-cover classification. *Photogrammetric Engineering and Remote Sensing*, *52*, 535–544.

Lunetta, R. S., & Balogh, M. (1999). Application of multi-temporal Landsat 5 TM imagery for wetland identification. *Photogrammetric Engineering and Remote Sensing*, *65*, 1303–1310.

Munro, D. C., & Touron, H. (1997). The estimation of marshland degradation in southern Iraq using multitemporal Landsat TM images. *International Journal of Remote Sensing*, *18*, 1597–1606.

Oregon Department of Agriculture [ODA]. (1999). *1997–1998 Oregon Agriculture and Fisheries Statistics*. Available at: http://www.oda.state.or.us/oass/con98.htm.

Panigrahy, S., & Sharma, S. A. (1997). Mapping of crop rotation using multidate Indian remote sensing satellite digital data. *ISPRS Journal of Photogrammetry and Remote Sensing*, *52*, 85–91.

Pax-Lenney, M., & Woodcock, C. E. (1997). Monitoring agricultural lands in Egypt with multitemporal Landsat TM imagery: how many images are needed? *Remote Sensing of Environment*, *59*, 522–529.

Pax-Lenney, M., Woodcock, C. E., Collins, J. B., & Hamdi, H. (1996). The status of agricultural lands in Egypt: the use of multitemporal NDVI features derived from Landsat TM. *Remote Sensing of Environment*, *56*, 8–20.

Plunk, D. E. Jr., Morgan, K., & Newland, L. (1990). Mapping impervious cover using Landsat TM data. *Journal of Soil and Water Conservation*, *45*, 589–591.

Pacific Northwest Ecosystem Research Consortium [PNW-ERC]. (2000). *The Pacific Northwest Ecosystem Research Consortium*. Available at: http://www.orst.edu/dept/pnw-erc/index.htm.

Ryerson, R. A., Dobbins, R. N., & Thibault, C. (1985). Timely crop area estimates from Landsat. *Photogrammetric Engineering and Remote Sensing*, *51*, 1735–1743.

San Miguel-Ayanz, J., & Biging, G. S. (1997). Comparison of single-stage and multi-stage classification approaches for cover type mapping with TM and SPOT data. *Remote Sensing of Environment*, *59*, 92–104.

Schriever, J. R., & Congalton, R. G. (1995). Evaluating seasonal variability as an aid to cover-type mapping from Landsat Thematic Mapper data in the Northeast. *Photogrammetric Engineering and Remote Sensing*, *61*, 321–327.

Shueb, S., & Atkins, P. (1991). Crop area estimation: a comparison of remote sensing and census methods. *Geography*, *76*, 235–239.

Towle, J. C. (1982). Changing geography of Willamette Valley woodlands. *Oregon Historical Quarterly*, *83*, 67–86.

Tuchmann, E. T., Connaughton, K. P., Freedman, L. E., & Moriwaki, C. B. (1996). *The Northwest Forest Plan: a report to the President and Congress*. Portland, OR: USDA Office of Forestry and Economic Assistance (253 pp.).

Turner, B. L. II, & Meyer, W. B. (1994). Global land-use and land-cover change: an overview. In: W. B. Meyer & B. L. Turner II (Eds.), *Changes in land use and land cover: a global perspective* (pp. 3–10). Cambridge: Cambridge Univ. Press.

Uhrich, M. A., & Wentz, D. A. (1999). *Environmental setting of Willamette Basin (water resources investigation report 97-4082-A)*. Portland, OR: USGS National Water Quality Assessment Program (20 pp.).

United States Department of Agriculture [USDA]. (1993). *Forest ecosystem management: an ecological, economic, and social assessment report of Forest Ecosystem Management Assessment Team*. Ogden, UT: USDA Forest Service.

Vogelmann, J. E. (1988). Detection of forest change in the Green Mountains of Vermont using multispectral scanner data. *International Journal of Remote Sensing*, *9*, 1187–1200.

Willamette Valley Livability Forum. (1999). *About the Willamette Livability Forum*. Available at: http://www.econ.state.or.us/wvlf/.

Williams, V. L., Philipson, W. R., & Philpot, W. D. (1987). Identifying vegetable crops with Landsat Thematic Mapper data. *Photogrammetric Engineering and Remote Sensing*, *53*, 187–191.

Wolter, P. T., Mladenoff, D. J., Host, G. E., & Crow, T. R. (1995). Improved forest classification in the Northern Lake States using multi-temporal Landsat imagery. *Photogrammetric Engineering and Remote Sensing*, *61*, 1129–1143.

Zhuang, X., Engel, B. A., Baumgardner, M. F., & Swain, P. H. (1991). Improving classification of crop residues using digital land ownership data and Landsat TM imagery. *Photogrammetric Engineering and Remote Sensing*, *57*, 1487–1492.